Journal of Constructional Steel Research 215 (2024) 108534

Contents lists available at ScienceDirect

Journal of Constructional Steel Research

journal homepage: www.elsevier.com/locate/jcsr

Axial compression behavior of coal gangue coarse aggregate concrete-filled steel tube stub columns

Jinli Wang [a,b,c], Yongxu Duan [a], Xuetao Lyu [d], Yang Yu [e,*], Jiaxuan Xiao [a]

[a] School of Civil Engineering, Liaoning Technical University, Fuxin 123000, China
[b] Key Laboratory of Coal Gangue Resource Utilization and Energy-Saving Building Materials in Liaoning Province, Fuxin 123000, China
[c] Engineering Research Center for Resource Utilization of Coal-Based Solid Waste in Liaoning Province, Fuxin 123000, China
[d] School of Transportation and Civil Engineering & Architecture, Foshan University, Foshan, Guangdong 528000, China
[e] Centre for Infrastructure Engineering and Safety, UNSW, Sydney, NSW 2052, Australia

ARTICLE INFO

Keywords:
Spontaneous-combustion coal gangue coarse aggregate (SCGCA)
Concrete-filled steel tube (CFST)
Axial compression tests
Analysis-oriented model

ABSTRACT

To investigate the load-strain curves and failure modes of spontaneous-combustion coal gangue coarse aggregate (SCGCA) concrete-filled steel tube (CFST) stub columns under axial compression, 36 SCGCA CFST specimens and 18 comparative SCGCA concrete specimens were firstly tested with various SCGCA replacement ratios, concrete strengths and steel tube thicknesses. The results reveal that the bearing capacity of SCGCA CFST significantly decreases with increasing SCGCA replacement ratio, while corresponding strain increases. The addition of SCGCA can activate confining stress offered by steel tube in advance. The hoop strain of SCGCA CFST specimens increases with increasing SCGCA replacement ratio under same axial strain, resulting in enhanced confining stress. An analysis-oriented model of SCGCA CFST stub columns was then established on basis of test results, and an extended parameter analysis was further conducted using the model. Finally, the feasibility of design methods in existing design codes for evaluating bearing capacity of SCGCA CFST stub columns under axial compression was discussed.

1. Introduction

To meet the requirements of economic and social development, annual consumption of coal resources in China has reached 40 million tons [1]. As the primary solid waste produced during the mining and processing of coal resources [2], the coal gangue in China has accumulated to 6 billion tons with annual increase of about 300–350 million tons [3]. This vast amount of coal gangue has led to a series of problems, including land appropriation and ecological destruction [4]. To address these issues, researchers have started exploring the potential substitution of coal gangue coarse aggregate (CGCA) for non-renewable natural coarse aggregate (NCA) in conventional structural concrete adopting relevant research approach [5–8]. For instance, Zhou et al. [9] introduced a compressive stress-strain model for CGCA concrete. Wang et al. [10] conducted experiments to study the influences of CGCA on mechanical behavior of concrete. Test results showed that the elastic modulus at 28 days reduced by 23% and 32% and the 360-day drying shrinkage increased by 62% and 92% for rock coal gangue coarse aggregate (RCGCA) concrete and spontaneous-combustion coal gangue coarse aggregate (SCGCA) concrete, respectively. They also recommended the drying shrinkage and elastic modulus predictive models for CGCA concrete [11,12]. Zhang et al. [13] carried out the tests to study the influences of particle size distribution and replacement ratio of SCGCA on mechanical behavior of concrete. The result demonstrated that compressive strength, splitting tensile strength and elastic modulus of concrete decreased by 19.4%, 36.1% and 32.2%, respectively, when SCGCA completely replaced NCA. The effect of coarse aggregate size distribution was found to be limited. Wang et al. [14] discussed the flexural behavior of concrete with NCA, SCGCA or SCGCA and coal gangue fine aggregate (CGFA) through experimental and numerical methods. Liu et al. [15] carried out both numerical and experimental studies on mechanical behavior of RCGCA concrete columns with various RCGCA replacement ratios and eccentricities. They further developed the design formulas for calculating bearing capacity of such column. Based on the current studies, it is evident that CGCA concrete has weaker workability and mechanical behavior than NCA concrete owing to high water absorption, porous properties and low crushing strength. Therefore, researchers have proposed the method of using

* Corresponding author.
E-mail address: yang.yu12@unsw.edu.au (Y. Yu).

https://doi.org/10.1016/j.jcsr.2024.108534
Received 14 November 2023; Received in revised form 27 January 2024; Accepted 5 February 2024
Available online 10 February 2024

Table 1
Specimen detail.

Specimens	Label	L (mm)	D (mm)	f_{cd} (MPa)	r (%)	t (mm)
SCGCA concrete	C40–0-1,2,3	300	150	40	0	/
	C40–50–1,2,3				50	/
	C40–100–1,2,3				100	/
	C60–0-1,2,3	300	150	60	0	/
	C60–50–1,2,3				50	/
	C60–100–1,2,3				100	/
SCGCA CFST	S40–0-a-1,2	450	156	40	0	3.0
	S40–50-a-1,2				50	
	S40–100-a-1,2				100	
	S40–0-b-1,2	450	158	40	0	4.0
	S40–50-b-1,2				50	
	S40–100-b-1,2				100	
	S40–0-c-1,2	450	159	40	0	4.5
	S40–50-c-1,2				50	
	S40–100-c-1,2				100	
	S60–0-a-1,2	450	156	60	0	3.0
	S60–50-a-1,2				50	
	S60–100-a-1,2				100	
	S60–0-b-1,2	450	158	60	0	4.0
	S60–50-b-1,2				50	
	S60–100-b-1,2				100	
	S60–0-c-1,2	450	159	60	0	4.5
	S60–50-c-1,2				50	
	S60–100-c-1,2				100	

external confinement to enhance mechanical properties of CGCA concrete [16–21], and the CGCA concrete-filled steel tube (CFST) has emerged as a solution to ease resource pressure, lower energy consumption [22–24], and further unlock the possibility of coal gangue as "green" building materials, aligning with the demands of the times.

Li et al. [25] and Li and Zhong [26] developed the strength criteria, constitutive relationship and transverse deformation coefficient of core concrete in SCGCA CFST stub column through combined experimental research and theoretical analysis. Gao et al. [20] conducted experiments to study the influence of RCGCA replacement ratio on axial mechanical behavior of RCGCA CFST stub column and proposed a revised design approach for such columns. Test and analysis results revealed that axial compressive strength and elastic modulus of specimens decreased with increasing RCGCA replacement ratio, suggesting that relatively lower concrete strength and higher steel strength were more suitable for RCGCA CFST stub columns. Meanwhile, Zhang et al. [21] conducted experimental and numerical studies to explore mechanical properties of SCGCA CFST stub column under axial compression, considering various SCGCA replacement ratios and steel tube thicknesses. They also provided recommended calculation formulae for determining bearing capacity of such columns.

Based on existing studies, it can be inferred that there is still limited theoretical and experimental research on the mechanical behavior of SCGCA CFST stub column. In addition, an analysis-oriented model of NCA CFST stub columns proposed by Kwan et al. [27] offered a new approach to predict mechanical behavior of SCGCA CFST stub columns under axial compression. Yu et al. [28] conducted experiments on CFST stub columns with different aggregate types and found that specimens made of lightweight concrete exhibited faster lateral expansion when contrasted with samples made of ordinary concrete. Accordingly, this research conducted axial compressive test on SCGCA CFST stub column, investigating the effects of SCGCA replacement ratio, steel tube thickness and concrete strength on load-strain curves and failure modes. Subsequently, an analysis-oriented model of SCGCA CFST stub columns was established, considering assumption of path independence, modified hoop strain-axial strain model and axial stress-axial strain model of core concrete, which was further verified through the comparison of axial load-axial strain curves and axial bearing capacity between predicted and tested results. Furthermore, the study examined the impact of critical parameters on mechanical behavior of SCGCA CFST stub column

Fig. 1. Diagram of SCGCA.

Table 2
Material properties of aggregates.

Material characteristics	SCGCA	NCA	NFA
Loose bulk density (kg/m^3)	978	1304	1457
Apparent density (kg/m^3)	2476	2664	2602
Tap bulk density (kg/m^3)	1114	1420	1565
Void content (%)	48.72	54.65	41.6
Moisture content (%)	0.83	2.56	0.64
Water absorption (%)	8.25	2.42	1.3
Particle size distribution (mm)	4.75–19.5	4.75–19.5	0.01–4.75
Crushing value (%)	16.5	5.83	/
Crushing strength (Mpa)	5.4	32.5	/

subjected to axial compression using the analysis-oriented model. The applicability of existing design formulas in evaluating bearing capacity of SCGCA CFST stub column under axial compression was discussed in relation to the comparison with tested and numerical results. The findings in this study can serve as a foundation for the application of SCGCA CFST as a structural member, further promoting the large-scale utilization of coal gangue resources.

2. Experimental program

2.1. Design of specimens

A total of 54 cylindrical specimens, including 36 SCGCA CFST stub columns and 18 SCGCA concrete ones as reference, were tested under axial compression. Table 1 lists the design details of specimens, where L is the height of specimens, D is the section diameter of SCGCA CFST and SCGCA concrete specimens, r represents the SCGCA replacement ratio of specimens, f_{cd} is the design compressive strength of SCGCA concrete with $r = 0$ (NCA concrete), t is the thickness of steel tube of SCGCA CFST specimens. The specimens are categorized as follows: letters "C" and "S" represent the SCGCA concrete specimens and SCGCA CFST specimens, respectively; the followed figures of 40 and 60 represent $f_{cd} = 40$ MPa and 60 MPa, respectively; the figures of 0, 50 and 100 in second part represent $r = 0$, 50% and 100% respectively; letters "a", "b" and "c" represent $t = 3.0$ mm, 4.0 mm and 4.5 mm respectively; and figure of 1, 2 and 3 in last part represent different specimens with identical parameters. For instance, the specimen labeled S60–50-b-2 is the second SCGCA CFST specimen with a design strength of 60 MPa for concrete, $r = 50\%$ and $t = 4.0$ mm.

2.2. Materials

2.2.1. SCGCA and NCA

The raw material of spontaneous-combustion coal gangue was secured from Fuxin, China and processed to the SCGCA with 4.75–19.5 mm continuous gradation (Fig. 1) through operations of crushing, screening, classification and mixing. The natural gravel with the same gradation as SCGCA and river sand with 0.01–4.75 mm particle size scale and 2.58 fineness modulus were used as natural coarse aggregate (NCA) and natural fine aggregate (NFA), respectively, which met

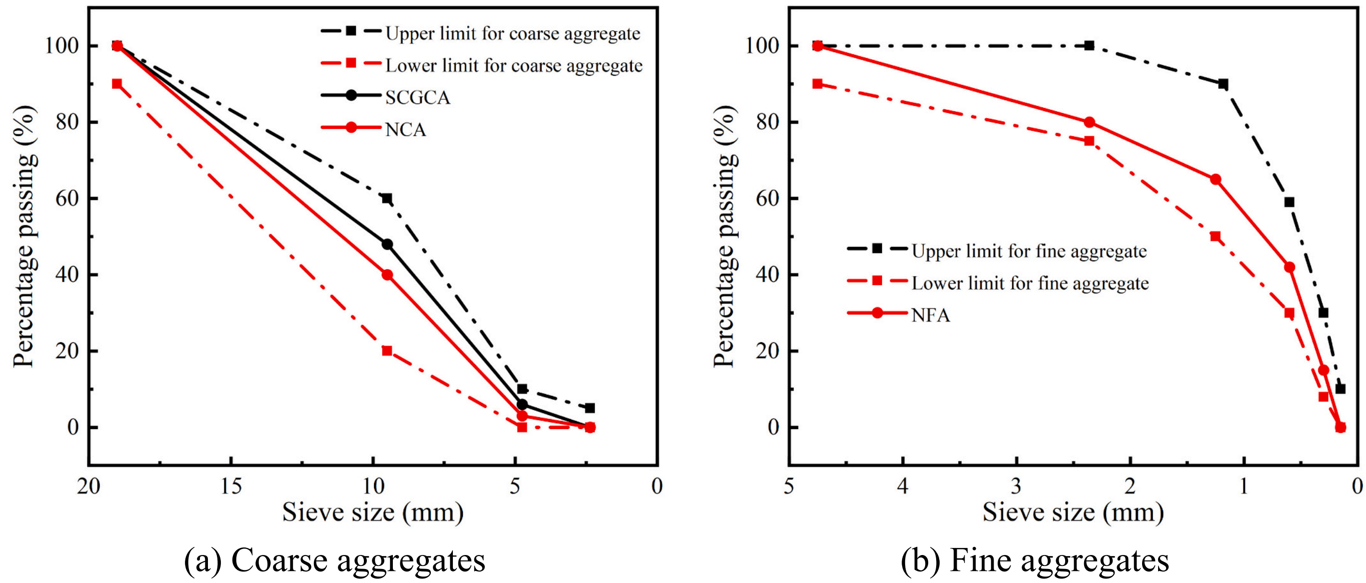

Fig. 2. Particle size distributions of coarse and fine aggregates.

Table 3
Main chemical constituents of SCGCA (%).

SiO_2	Al_2O_3	Fe_2O_3	MgO	CaO	K_2O	Na_2O	TiO_2	P_2O_5	SO_3	Cl	MnO
57.46	18.66	7.06	2.54	3.61	3.98	1.86	0.90	0.23	0.75	0.12	2.75

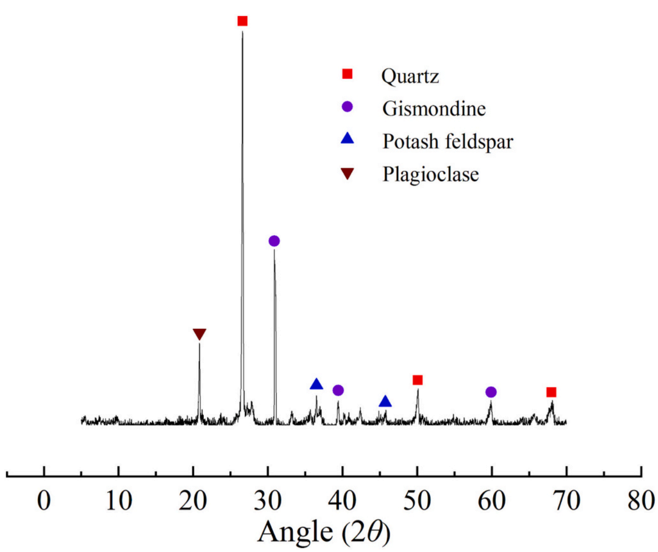

Fig. 3. XRD spectra of SCGCA.

requirements of particle size distribution of aggregates in JGJ 52–2006 [29]. The material properties of SCGCA, NCA and NFA were tested according to the methods specified for normal concrete in JGJ 52–2006 [20] and relevant values are given in Table 2. Particle size distributions of SCGCA, NCA and NFA are portrayed in Fig. 2, meeting requirements of GB/T 14685–2011 [30] and GB/T 14684–2011 [31].

To explore chemical compositions and physical phases of SCGCA, X-ray diffraction (XRD) and X-ray fluorescence (XRF) tests were respectively conducted on its powder of concrete with a compressive strength of 39.6 MPa. The XRF analysis result is displayed in Table 3 and it is noticeable that SiO_2 (57.46%) and Al_2O_3 (18.66%) are the major chemical constituents of SCGCA, similar to that of the NCA. The XRD spectra results are shown in Fig. 3 and it can be seen that quartz and gismondine are the main mineral constituents of SCGCA.

Table 4
Material properties of steel tubes.

Type	$D \times t$ (mm × mm)	f_y (Mpa)	f_u (Mpa)	E_s (Gpa)	ν_s
1	156 × 3.0	282	459	201	0.28
2	158 × 4.0	295	465	206	0.28
3	159 × 4.5	317	477	204	0.29

2.2.2. Steel

There were three types of steel tube in SCGCA CFST specimens. Three standard coupons cut from the longitudinal portion were prepared for each type of steel tube. Material properties of steel tube were obtained through the tensile test of standard coupons based on the methods recommended in GB/T 228.1–2021 [32] and the average values of that are listed in Table 4, in which f_u denotes the tensile (ultimate) strength, f_y represents yield strength, E_s denotes modulus of elasticity, and ν_s denotes Poisson's ratio.

2.2.3. Concrete

There were six types of concrete in specimens. The mixture of concrete was designed according to JGJ 55–2011 [33] and the materials used were NCA, SCGCA, NFA, tap water in laboratory, P·O 42.5 cement and a high-efficiency water reducer with a reduced rate of 30%. The amount of SCGCA in concrete with different *r* was determined on basis of the fundamental of replacing NCA with equal volume and pre-wetting of one hour was required for SCGCA due to high water absorption and large porosity of that. The additional water usage was 60% of the water absorption of SCGCA to guarantee that the mixture of concrete met related construction requirement [34]. The mix proportions, slump and 28-day cubic compressive strength (f_{cu}) of concrete are recorded in Table 5.

Table 5
Mixture, slump and compressive strength of concrete.

Type	r (%)	Raw materials (kg/m^3)							Slump (mm)	f_{cu} (Mpa)
		NCA	SCGCA	NFA	Water	Cement	Water reducer	Additional water		
40–0	0	1024	/	627	188	470	9.4	0	95	49.2
40–50	50	512	476	627	188	470	9.4	37	90	39.6
40–100	100	/	952	627	188	470	9.4	74	75	30.4
60–0	0	1031	/	605	172	520	10.4	0	115	65.8
60–50	50	515	479	605	172	520	10.4	37	105	52.5
60–100	100	/	958	605	172	520	10.4	74	85	39.4

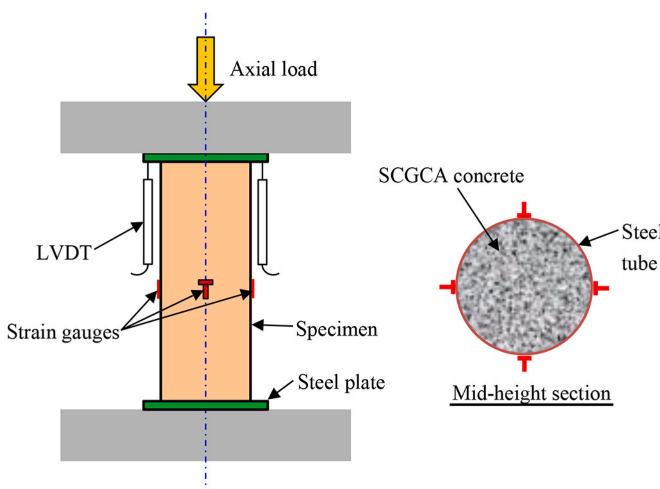

Fig. 4. Test set-up and instrumentation arrangement.

2.3. Specimen preparation

The plastic molds with the diameter of 150 mm and the height of 300 mm and steel tubes with the internal diameter of 150 mm and the height of 450 mm were fabricated for t SCGCA concrete and SCGCA CFST, specimens respectively. The debris on inner and outer surfaces of plastic molds and steel tubes were cleaned before pouring concrete. Besides that, the rust on inner and outer surfaces of steel tube were wire brushed off and then a steel plate with the dimension of 160 mm × 160 mm × 10 mm was welded beneath it. The concrete was poured into the vertically-placed plastic molds and steel tubes, vibrated until fully consolidated and wrapped tightly with plastic film. After curing under standard condition ($RH \geq 95\%$, $T = 20 \pm 2$ °C) for 28 days, the top of each specimen was polished to obtain the smooth surface. For SCGCA CFST specimens, another steel plate with the same size was welded onto the top of steel tube to gurantee that core concrete and steel tube worked together during initial loading phase.

2.4. Instrumentation and test method

The tests of SCGCA concrete and SCGCA CFST specimens under axial compression were conducted using 5000 kN hydraulic compression machine, and the load and measurement devices are depicted in Fig. 4. Four pairs of strain gauges were mounted at the mid-height of each specimen, with each pair of strain gauges positioned at 90° intervals. The longitudinal and circumferential strain gauges were used to obtain the axial and hoop strains of the specimens, respectively. Furthermore, two linear variable differential transformers (LVDTs) were symmetrically arranged to measure the axial displacement of the specimens. The preload tests and alignment validation were implemented prior to formal loading. The tests were stably controlled by a loading rate of 1 mm/min and terminated when the axial displacement reached 20 mm.

3. Results and discussion

3.1. SCGCA CFST specimens

3.1.1. Failure modes

The failure modes of the SCGCA CFST and concrete specimens are shown in Fig. 5. It can be seen that, for SCGCA concrete specimens, the failure modes gradually transform from shear failure to longitudinal splitting with the increasing r. For SCGCA CFST specimens, outward buckling occurred at the end and mid-height of the steel tubes; the specimens with larger t (e.g., S40–50-c) displayed drum-like failure while those with smaller t (e.g., S40–50-a) exhibited typical shear failure; moreover, the inner concrete remained good integrity apart from the crushing happened at the position of outward buckling; the specimens with larger r showed more obvious damage of the core concrete and greater outward buckling of the steel tube.

3.1.2. Axial load-axial strain and corresponding hoop strain-axial strain relationship

Table 6 records the mechanical indexes of the SCGCA CFST and concrete specimens, where N_{us} and N_{uc} are the bearing capacity of the SCGCA CFST and concrete specimens, respectively; The peak stress (f_{co}) and elastic modulus (E_{co}) of SCGCA concrete specimens are determined according to the specific method in GB/T 50081–2019 [35]; ε_{cc} and ε_{co} are the peak strains at N_{us} and N_{uc}, respectively; ε_{csc} and ε_{sc} are respectively the axial splitting strain of the SCGCA CFST and concrete specimens, which is the indicator of forming splitting cracks in concrete. It should be noted that the formation of splitting cracks is a sign that the concrete has created the inelastic hoop strain [30]. Since the confinement effect of steel tube to core concrete is passive, the confining stress of the steel tube affects the hoop strain of the core concrete, and vice versa [27]. Therefore, it is crucial to obtain the mechanical behavior of the SCGCA CFST specimens by accurately estimating the hoop strain of the core concrete and confining stress of the steel tube.

Fig. 6 depicts the effects of r and t on axial load-axial strain curves and corresponding hoop strain-axial strain curves of SCGCA CFST specimen, in which N denotes axial load imposed on thspecimens; ε_z and ε_h represent axial and hoop strains, respectively; ε_z and ε_h are taken as the positive and negative values respectively, which remains consistent throughout the subsequent analysis; the blue squares and green triangles respectively are the elastic limit point of ε_h-ε_z curve and peak point of N-ε_z curve, which are respectively represented by ε_{csc} and ε_{cc} for the SCGCA CFST specimens. It can be found from the experiment that there is a similar changing trend in N-ε_z curves of two types of specimens. Thus, the SCGCA CFST specimens were taken as an example:

The whole N-ε_z curve of SCGCA CFST specimen can be categorized into three stages: (a) Elastic stage ($\varepsilon_z \in (0, \varepsilon_{csc}]$): when $\varepsilon_z \leq \varepsilon_{sc}$, steel tube and core concrete are in a separated state with no interaction between them; and when $\varepsilon_{sc} < \varepsilon_z \leq \varepsilon_{csc}$, the steel tube begins to confine core concrete as circumferential expansion of core concrete increases. In this stage, the concrete is always in the elastic stage because that confining stress can postpone the formation and development of the splitting cracks in core concrete. (b) Elastic-plastic stage ($\varepsilon_z \in (\varepsilon_{csc}, \varepsilon_{cc}]$): the axial strain enters elastic-plastic stage with the occurrence of splitting cracks

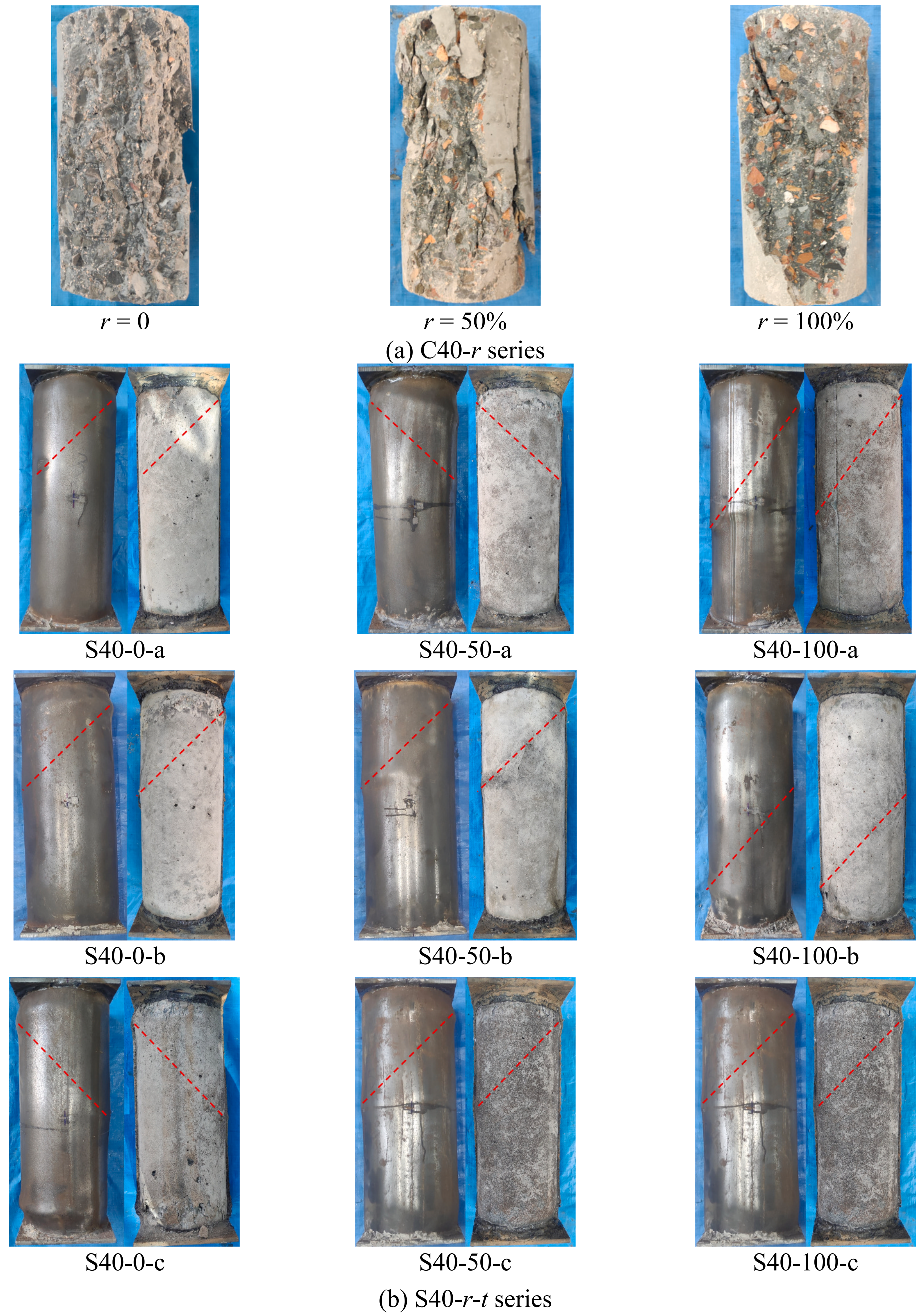

Fig. 5. The failure modes of SCGCA CFST and concrete specimens.

in core concrete. (c) Plastic stage ($\varepsilon_z \in (\varepsilon_{cc}, \infty)$): the axial strain enters plastic stage as axial load ascends to bearing capacity. The hoop strain-axial strain curves of specimens can be categorized into two stages: (a) $\varepsilon_z \in (0, \varepsilon_{csc}]$: the axial strain is small and the hoop one grows slowly; (b) $\varepsilon_z \in (\varepsilon_{csc}, \infty)$, the hoop strain enters the inelastic stage with the appearance of splitting cracks in core concrete, and at this stage, the hoop strain increases rapidly with increasing axial strain.

The following phenomenon can be observed in Fig. 6 and Table 6 for SCGCA CFST specimens:

(1) There is a downward trend for N_{us} with the increase of *r*. Specifically, the average value of N_{us} for S40–100-a series specimens and S60–100-a series specimens are 22.4% and 21.9% lower than that of N_{us} for S40–0-a series specimens and S60–0-a series specimens, respectively. It can be explained by the fact that compressive strength of core concrete decreases with increasing *r*, and the similar conclusion can be found in [36].

(2) There is also a downward trend for ε_{csc} with the increase of *r*. Specifically, the average value of ε_{csc} for S40–100-a series specimens and S60–100-a series specimens are 23.8% and 23.0% lower than that of ε_{csc} for S40–0-a series specimens and S60–0-a series specimens, respectively, which can be illustrated by earlier micro-cracks and circumferential expansion of specimens with the more SCGCA. Such unique characteristic can be used to activate confining stress offered by steel tube in advance.

(3) There is an upward trend for ε_{cc} with the increase of *r*. Specifically, the average value of ε_{cc} for S40–100-a series specimens and S60–100-a series specimens are 24.6% and 54.0% higher than that of ε_{cc} for S40–0-a series specimens and S60–0-a series specimens, respectively.

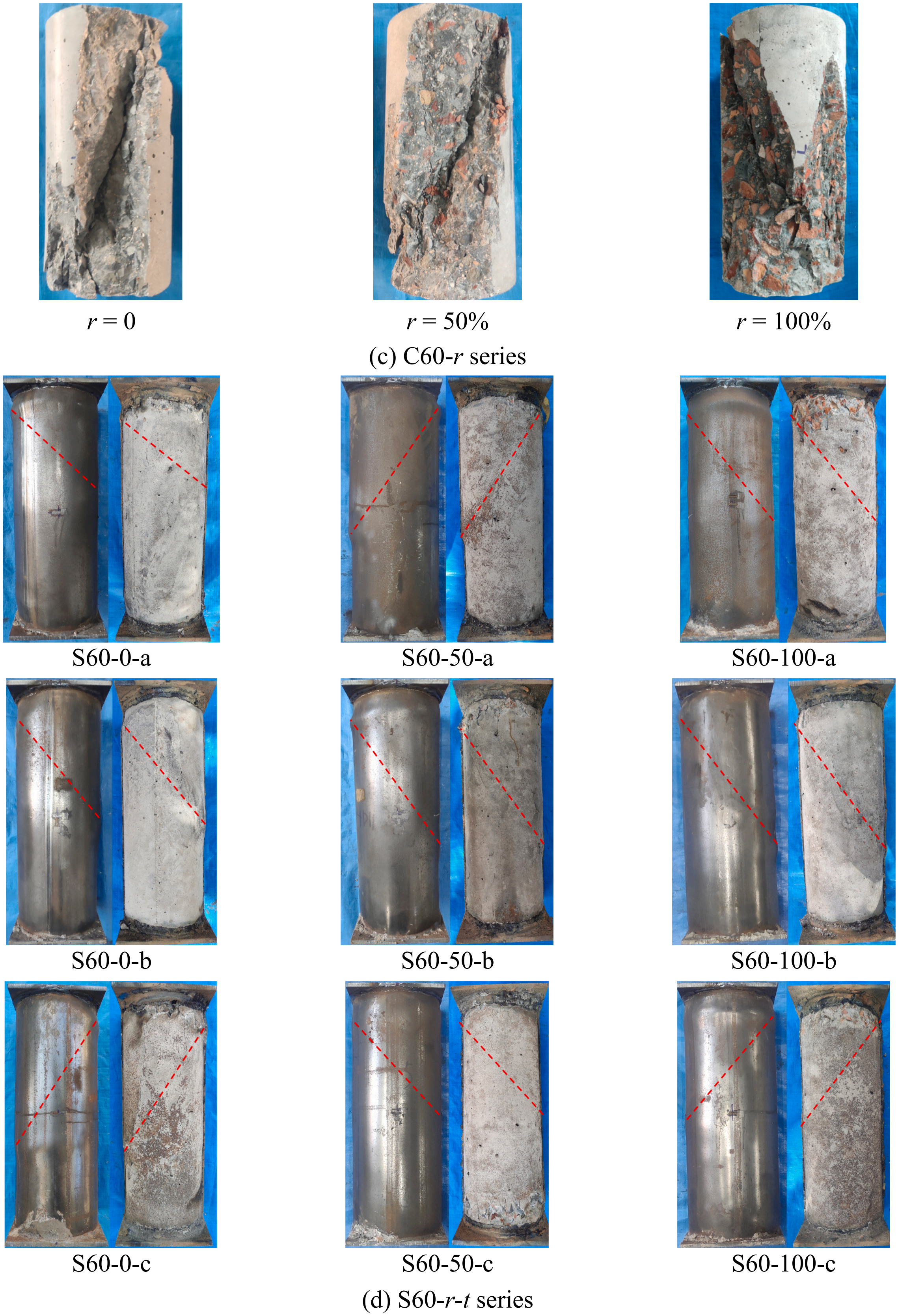

Fig. 5. (*continued*).

(4) The ε_h of SCGCA CFST specimens increases with increasing r at the same ε_z, which suggests that the addition of SCGCA causes a greater circumferential expansion of concrete. The confining stress of steel tube is passively applied to core concrete owing to the circumferential expansion of concrete. Therefore, the higher confining stresses can form with the greater circumferential

Table 6
The mechanical indexes of the SCGCA CFST and concrete specimens.

Specimens	r (%)	t (mm)	ε_{csc} (%)		ε_{cc} (%)		N_{us} (kN)		ε_{sc}	ε_{co}	N_{uc}	f_{co}	E_{co}	$\varepsilon_{cc}/\varepsilon_{co}$		N_{us}/N_{uc}	
			Value	Avg.	Value	Avg.	Value	Avg.	(%)	(%)	(kN)	(MPa)	(MPa)	Value	Avg.	Value	Avg.
S40–0-a-1	0	3	0.174	0.168	0.976	0.952	1561.9	1548.7	0.116	0.186	719.2	40.7	29,142	5.16	5.04	2.17	2.15
S40–0-a-2	0	3	0.162		0.928		1535.6							4.91		2.14	
S40–50-a-1	50	3	0.140	0.149	1.154	1.097	1319.0	1327.2	0.098	0.211	651.4	36.9	25,375	5.66	5.38	2.02	2.04
S40–50-a-2	50	3	0.158		1.040		1335.3							5.10		2.05	
S40–100-a-1	100	3	0.133	0.128	1.134	1.186	1191.9	1201.5	0.081	0.227	505.6	28.6	20,747	5.09	5.32	2.36	2.38
S40–100-a-2	100	3	0.123		1.238		1211.1							5.55		2.40	
S40–0-b-1	0	4	0.193	0.181	1.206	1.151	1764.7	1816.9	0.116	0.186	719.2	40.7	29,142	6.38	6.09	2.45	2.53
S40–0-b-2	0	4	0.169		1.096		1869.2							5.80		2.60	
S40–50-b-1	50	4	0.170	0.162	1.209	1.257	1665.8	1659.4	0.098	0.211	651.4	36.9	25,375	5.93	6.16	2.56	2.55
S40–50-b-2	50	4	0.154		1.305		1653.0							6.40		2.54	
S40–100-b-1	100	4	0.139	0.143	1.358	1.378	1385.4	1368.6	0.081	0.227	505.6	28.6	20,747	6.09	6.18	2.74	2.71
S40–100-b-2	100	4	0.147		1.398		1351.7							6.27		2.67	
S40–0-c-1	0	4.5	0.191	0.202	1.192	1.233	1910.4	1893.4	0.116	0.186	719.2	40.7	29,142	6.31	6.52	2.66	2.63
S40–0-c-2	0	4.5	0.213		1.274		1876.5							6.74		2.61	
S40–50-c-1	50	4.5	0.179	0.184	1.380	1.338	1701.3	1718.2	0.098	0.211	651.4	36.9	25,375	6.76	6.56	2.61	2.64
S40–50-c-2	50	4.5	0.189		1.296		1735.2							6.35		2.66	
S40–100-c-1	100	4.5	0.168	0.162	1.433	1.427	1519.2	1540.9	0.081	0.227	505.6	28.6	20,747	6.43	6.40	3.00	3.05
S40–100-c-2	100	4.5	0.156		1.421		1562.6							6.37		3.09	
S60–0-a-1	0	3	0.179	0.183	0.715	0.724	1812.5	1819.4	0.125	0.190	900.1	51.0	32,270	3.80	3.85	2.01	2.02
S60–0-a-2	0	3	0.187		0.733		1826.3							3.90		2.03	
S60–50-a-1	50	3	0.175	0.164	0.797	0.830	1605.3	1630.3	0.104	0.222	840.9	47.6	29,104	4.05	4.21	1.91	1.94
S60–50-a-2	50	3	0.153		0.863		1655.3							4.38		1.97	
S60–100-a-1	100	3	0.149	0.141	1.164	1.115	1410.5	1420.1	0.095	0.234	670.4	37.9	22,345	5.20	4.98	2.10	2.12
S60–100-a-2	100	3	0.133		1.066		1429.6							4.76		2.13	
S60–0-b-1	0	4	0.217	0.203	0.894	0.916	1995.3	1976.3	0.125	0.190	900.1	51.0	32,270	4.76	4.87	2.22	2.20
S60–0-b-2	0	4	0.189		0.928		1957.4							4.94		2.17	
S60–50-b-1	50	4	0.186	0.189	0.964	1.033	1851.0	1865.7	0.104	0.222	840.9	47.6	29,104	4.89	5.24	2.20	2.22
S60–50-b-2	50	4	0.192		1.102		1880.3							5.59		2.24	
S60–100-b-1	100	4	0.152	0.168	1.169	1.192	1688.9	1672.2	0.095	0.234	670.4	37.9	22,345	5.22	5.32	2.52	2.49
S60–100-b-2	100	4	0.184		1.215		1655.5							5.42		2.47	
S60–0-c-1	0	4.5	0.235	0.220	0.983	1.013	2175.8	2159.6	0.125	0.190	900.1	51.0	32,270	5.23	5.39	2.42	2.40
S60–0-c-2	0	4.5	0.205		1.043		2143.3							5.55		2.38	
S60–50-c-1	50	4.5	0.208	0.207	1.059	1.102	2032.1	2039.1	0.104	0.222	840.9	47.6	29,104	5.38	5.59	2.42	2.43
S60–50-c-2	50	4.5	0.206		1.145		2046.2							5.81		2.43	
S60–100-c-1	100	4.5	0.212	0.188	1.308	1.266	1792.6	1812.0	0.095	0.234	670.4	37.9	22,345	5.84	5.65	2.67	2.70
S60–100-c-2	100	4.5	0.164		1.224		1831.4							5.46		2.73	

expansion of concrete, which is capable of improving the ductility and strength of the structure [37].

(5) It can be found that with the increase of t, there are higher N_{us}, ε_{csc} and ε_{cc} under the same f_{cd} and r. The value of N_{us}/N_{uc} and $\varepsilon_{cc}/\varepsilon_{co}$ for specimens range from 1.94 to 3.05 and 3.85 to 6.56, respectively. In especial, when $t = 4.0$ mm, the value of N_{us}/N_{uc} for S40 and S60 series specimens range from 2.53 to 2.71 and 2.20 to 2.49 respectively and that of $\varepsilon_{cc}/\varepsilon_{co}$ for S40 and S60 series ones range from 6.09 to 6.18 and 4.87 to 5.32 respectively; when $f_{cd} = 60$ MPa, the value of N_{us}/N_{uc} for $t = 4.0$ mm and 4.5 mm series specimens range from 2.20 to 2.49 and 2.40 to 2.70 respectively and that of $\varepsilon_{cc}/\varepsilon_{co}$ for $t = 4.0$ mm and 4.5 mm series ones range from 4.87 to 5.32 and 5.39 to 5.65 respectively. Based on that, it can be concluded that the greater t and lower f_{cd} of the SCGCA CFST specimens, the better the enhancement effect of strength and ductility of those. Furthermore, under same axial strain, the hoop strain increases with decreasing t, which is consistent with the conclusions in Lai and Ho [38].

4. Analysis-oriented model for SCGCA CFST specimens

The research results in Kwan et al. [27] indicated that the essential ingredients for establishing the analysis-oriented model of SCGCA CFST specimens were as follows: (1) a confining stress-hoop strain model considering stress-strain characteristics of steel tube; (2) a hoop strain-axial strain model of core concrete considering different compressive strengths and confining stresses; (3) an axial stress-axial strain model of core concrete considering different compressive strengths and confining stresses.

4.1. Proposed analysis-oriented model

4.1.1. Stress-strain model of steel tube

In monotonic axial compression tests, the thin-walled steel tube of SCGCA CFST specimens is approximatively under a biaxial stress state with longitudinal compression ($\sigma_{z,s}$) and circumferential tension ($\sigma_{\theta,s}$), and its stress can be expressed as [39]:

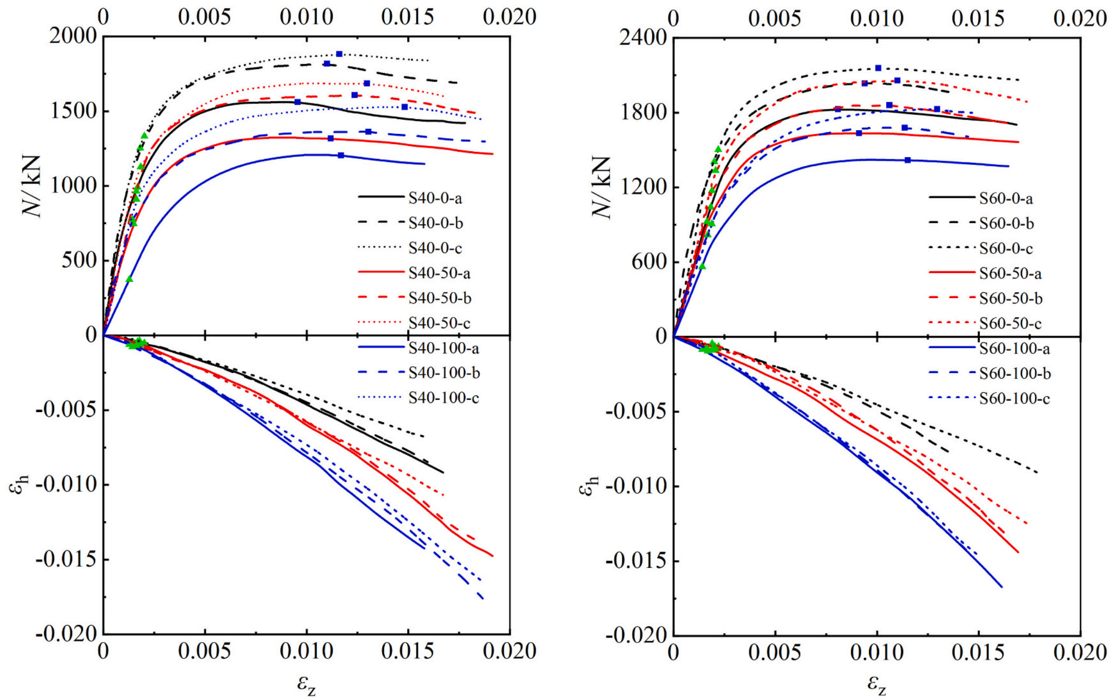

(a) f_{cd}=40 MPa (b) f_{cd}=60 MPa

Fig. 6. Effect of r and t on axial load-axial strain and hoop strain-axial strain curves of SCGCA CFST specimen.

$$\sigma_e = \sqrt{\sigma_{z,s}^2 - \sigma_{z,s}\sigma_{\theta,s} + \sigma_{\theta,s}^2} \tag{1}$$

For the stress of steel tube in elastic stage ($\sigma_e < f_y$), generalized Hooke's law is applied and expressed as:

$$\begin{bmatrix} d\sigma_{z,s}^i \\ d\sigma_{\theta,s}^i \end{bmatrix} = \frac{E_s}{1-v_s}\begin{bmatrix} 1 & v_s \\ v_s & 1 \end{bmatrix}\begin{bmatrix} d\varepsilon_{z,s}^i \\ d\varepsilon_{\theta,s}^i \end{bmatrix} \tag{2}$$

where $d\sigma_{z,s}^i$ and $d\sigma_{\theta,s}^i$ are the longitudinal and circumferential incremental stresses respectively, $d\varepsilon_{z,s}^i$ and $d\varepsilon_{\theta,s}^i$ are the longitudinal and circumferential incremental strains respectively, and i denotes the number of incremental steps.

For the stress of steel tube in plastic stage ($\sigma_e \geq f_y$), incremental Prandtl-Reuss equation is utilized and expressed as:

$$\begin{bmatrix} d\sigma_{z,s}^i \\ d\sigma_{\theta,s}^i \end{bmatrix} = \frac{E_s}{1-v_s}\begin{bmatrix} 1-\dfrac{s_a^2}{s_c} & v_s-\dfrac{s_a s_b}{s_c} \\ v_s-\dfrac{s_a s_b}{s_c} & 1-\dfrac{s_b^2}{s_c} \end{bmatrix}\begin{bmatrix} d\varepsilon_{z,s}^i \\ d\varepsilon_{\theta,s}^i \end{bmatrix} \tag{3}$$

where $s_a = s_x + v_s s_\theta$, $s_b = v_s s_x + s_\theta$, $s_c = s_x^2 + s_\theta^2 + v_s s_x$; and $s_x = \frac{1}{3}\left(2\sigma_{z,s}^{i-1} - \sigma_{\theta,s}^{i-1}\right)$, $s_\theta = \frac{1}{3}\left(-\sigma_{z,s}^{i-1} + 2\sigma_{\theta,s}^{i-1}\right)$.

4.1.2. Hoop strain-axial strain model of core concrete

Fig. 7 depicts the comparison of the hoop strain (ε_h)-axial strain (ε_z) curves of core concrete in SCGCA CFST specimens between the calculated results by Kwan et al. [21] and the tested results, where the blue and black lines represent the calculated and tested results respectively. It is noticeable that hoop strain in the tested curves is greater than that in Kwan's model under the same axial strain, which indicates that hoop strain-axial strain model of NCA concrete presented in Kwan et al. [27] isn't suitable for the core concrete in SCGCA CFST specimens.

The model in Chen et al. [40] is modified by considering the influence of r based on tested results of SCGCA concrete specimens to demonstrate mechanical properties of those specimens, which can be expressed as:

$$f_{co} = \left(1 + 0.018r - 0.302r^2\right)f_{co}' \tag{4}$$

$$\varepsilon_{co} = (1 + 0.26r)\varepsilon_{co}' \tag{5}$$

$$E_{co} = (1 - 0.32r)E_{co}' \tag{6}$$

where $E_{co}' = 4700\sqrt{f_{co}'}$, $\varepsilon_{co}' = 700 + 172\sqrt{f_{co}'}$, f_{co} and ε_{co} denote peak stress and corresponding strain of SCGCA concrete specimens respectively, f_{co}' and ε_{co}' denote peak stress and corresponding strain of NCA concrete specimens respectively, E_{co} and E_{co}' denote elastic modulus of SCGCA concrete and NCA concrete specimens.

Thus, the model in Kwan et al. [27] is modified by considering the effect of r to portray hoop strain-axial strain relationship of core concrete in SCGCA CFST specimens, which can be expressed as:

$$\varepsilon_x^e = -v_c\varepsilon_z^T + \left(1 - v_c - 2v_c^2\right)\frac{\sigma_r}{E_{co}} \tag{7}$$

$$\varepsilon_x^p = -19.1k_1\left(\varepsilon_z^T - \varepsilon_{csc}\right)^{1.5}\left\{0.1 + 0.9\left[exp\left(-5.3k_2\left(\frac{\sigma_r}{f_{co}}\right)^{1.1}\right)\right]\right\} \tag{8}$$

$$\frac{\varepsilon_{csc}}{\varepsilon_{co}} = \left(0.44 + 0.0021f_{co} - 0.00001f_{co}^2\right)\left(1 + 30exp(-0.013f_{co})\frac{\sigma_r}{f_{co}}\right) \tag{9}$$

$$\varepsilon_x^T = \varepsilon_x^e + \varepsilon_x^p \tag{10}$$

where ε_x^e and ε_x^p denote elastic and inelastic hoop strains of core concrete in SCGCA CFST specimens respectively, ε_x^T and ε_z^T denote hoop and axial strains of core concrete in SCGCA CFST specimens respectively, v_c is the Poisson's ratio of SCGCA concrete specimens and taken as 0.2 herein, σ_r is confining stress of steel tube to core concrete in SCGCA CFST specimens, ε_{csc} denotes axial splitting strain of SCGCA CFST concrete specimens, k_1 and k_2 are calculating coefficients considering r.

Before the formation of splitting cracks, the concrete is under elas-

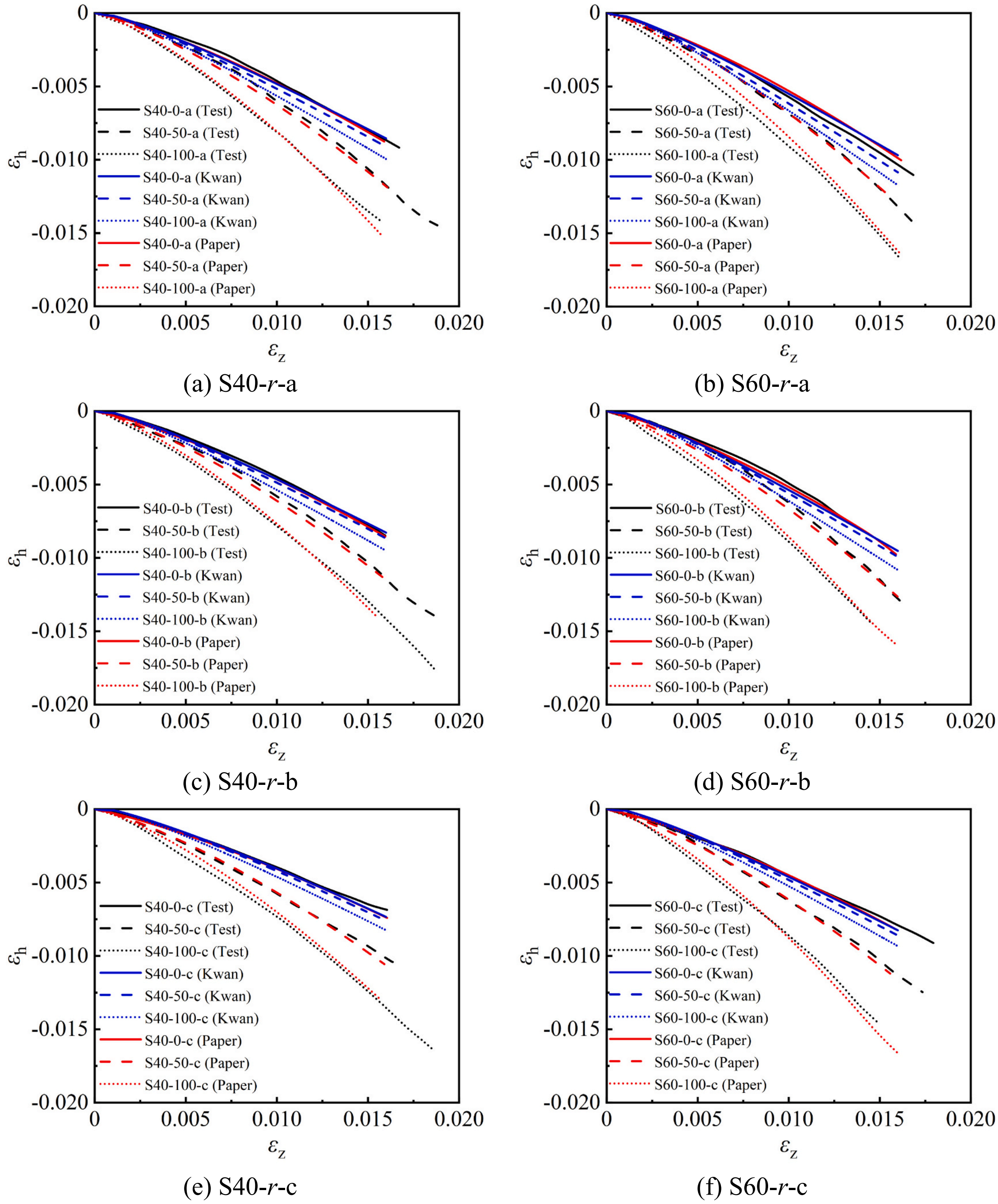

Fig. 7. Comparison of hoop strain-axial strain curves between calculated and tested results.

ticity and isotropy, and at this time, the elastic hoop strain (ε_x^e) is calculated according to Eq. (7). After the formation of splitting cracks, the concrete is inelastic and anisotropic and hoop strain (ε_x^T) is the sum of elastic strain caused by Poisson's effect and inelastic one caused by splitting cracks, as shown in Eq. (10).

In order to determine the calculation methods of k_1 and k_2, it is assumed that the bond between concrete and steel tube is intact [38] and these two components meet the deformation coordination conditions under axial compression, which can be denoted as:

$$\varepsilon_x^T = \varepsilon_{\theta,s} = \varepsilon_h \tag{11}$$

$$\varepsilon_z^T = \varepsilon_{z,s} = \varepsilon_z \tag{12}$$

Then, based on the regression analysis of the ahead tested ε_h-ε_z curves of SCGCA CFST specimens, the calculation methods of k_1 and k_2 are as follows:

$$k_1 = 1 + 0.25r^2 \tag{13}$$

$$k_2 = 1 - 0.21r^2 \tag{14}$$

The comparison of hoop strain (ε_h)-axial strain (ε_z) curves of core concrete in SCGCA CFST specimens between the calculated results by Eqs. (7)–(10) and the tested results is shown in Fig. 7, where the red and black lines represent the calculated and tested results respectively. It can be concluded that the modified model in the paper offers a more reasonable prediction of hoop strain-axial strain relationship of core concrete in SCGCA CFST specimens compared to Kwan's model.

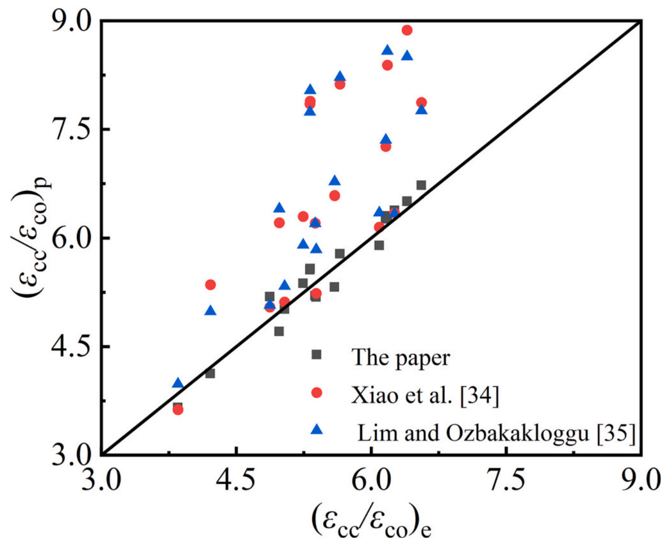

Fig. 8. Comparison of peak strain ratios between test results and model predictions.

4.1.3. Axial stress-axial strain model of core concrete

Scholars have proposed several confined concrete models [41–44], including analysis models that consider stress-path dependence [45–47] and active confinement models. The models developed in Attard and Setunge [48] and Xiao et al. [49] are applied to characterize axial stress-axial strain relationship of core concrete in SCGCA CFST specimen and formulated as:

$$\frac{\sigma_z^T}{f_{cc}} = \frac{A\left(\frac{\varepsilon_z^T}{\varepsilon_{cc}}\right) + B\left(\frac{\varepsilon_z^T}{\varepsilon_{cc}}\right)^2}{1 + (A-2)\left(\frac{\varepsilon_z^T}{\varepsilon_{cc}}\right) + (B+1)\left(\frac{\varepsilon_z^T}{\varepsilon_{cc}}\right)^2} \tag{15}$$

$$\frac{f_{cc}}{f_{co}} = 1 + 3.24\left(\frac{\sigma_r}{f_{co}}\right)^{0.80} \tag{16}$$

where σ_z^T is axial strain of core concrete in SCGCA CFST specimens, f_{cc} and ε_{cc} denote maximum stress and corresponding strain of core concrete in SCGCA CFST specimens respectively, A and B denote factors controlling the shape of axial stress-axial strain curve and expressed as:

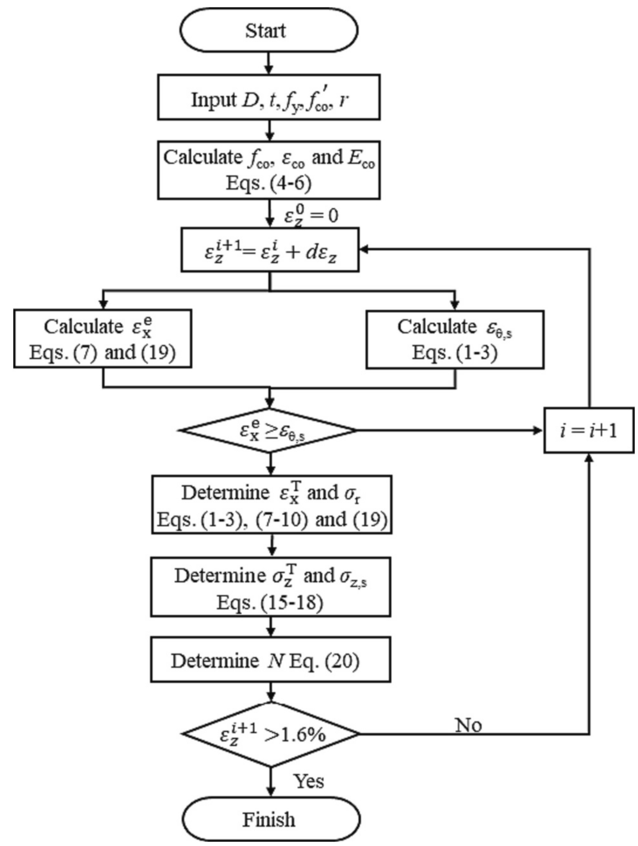

Fig. 9. Flowchart of the analysis process.

$$\begin{cases} A = \dfrac{E_c \varepsilon_{cc}}{f_{cc}}, B = \dfrac{(A-1)^2}{0.55} \text{ ascending portion} \\ A = \left[\dfrac{\varepsilon_{2i} - \varepsilon_i}{\varepsilon_{cc}}\right]\left[\dfrac{\varepsilon_{2i}\left(\frac{f_i}{\varepsilon_i}\right)}{(f_{cc} - f_i)} - \dfrac{4\varepsilon_i\left(\frac{f_{2i}}{\varepsilon_{2i}}\right)}{(f_{cc} - f_{2i})}\right], B = (\varepsilon_i - \varepsilon_{2i})\left[\dfrac{\left(\frac{f_i}{\varepsilon_i}\right)}{(f_{cc} - f_i)} - \dfrac{4\left(\frac{f_{2i}}{\varepsilon_{2i}}\right)}{(f_{cc} - f_{2i})}\right] \text{ descending portion} \end{cases} \tag{17}$$

where $\frac{\varepsilon_i}{\varepsilon_{cc}} = \frac{(2.50 - 0.30 ln(f_{co}) - 2}{1.12\left(\frac{\sigma_r}{f_{co}}\right)^{0.26} + 1} + 2$, $\frac{f_i}{f_{cc}} = \frac{(1.47 - 0.17 ln(f_{co}) - 1}{5.06\left(\frac{\sigma_r}{f_{co}}\right)^{0.57} + 1} + 1$, $\varepsilon_{2i} = (2\varepsilon_i - \varepsilon_{cc})$, $\frac{f_{2i}}{f_{cc}} = \frac{(1.45 - 0.25 ln(f_{co}) - 1}{6.35\left(\frac{\sigma_r}{f_{co}}\right)^{0.62} + 1} + 1$.

Fig. 8 plots the comparison of $\varepsilon_{cc}/\varepsilon_{co}$ of specimens between the predicted results by Xiao et al. [49] and Lim and Ozbakakloggu [50] and the tested results, where $(\varepsilon_{cc}/\varepsilon_{co})_e$ and $(\varepsilon_{cc}/\varepsilon_{co})_p$ are the tested and predicted results respectively. It is noted that existing peak strain models of NCA concrete in Xiao et al. [49] and Lim and Ozbakakloggu [50] aren't applicable to SCGCA CFST specimens.

To obtain the reliable $\varepsilon_{cc}/\varepsilon_{co}$, a modified equation based on Xiao et al. [49] is suggested, which considering the effect of r.

$$\frac{\varepsilon_{cc}}{\varepsilon_{co}} = 1 + 17.4a\left(\frac{\sigma_r}{f_{co}}\right)^{1.06b} \tag{18}$$

where $a = 1 - 0.168r$, $b = 1 - 0.13r + 0.72r^2$.

The comparison of $\varepsilon_{cc}/\varepsilon_{co}$ of specimens between the predicted results by Eq. (18) and the tested results is displayed in Fig. 8, where $(\varepsilon_{cc}/\varepsilon_{co})_e$ and $(\varepsilon_{cc}/\varepsilon_{co})_p$ are the tested and predicted results respectively. It can be concluded that the mean value (MV), standard deviation (SD) and average absolute error (AAE) of $(\varepsilon_{cc}/\varepsilon_{co})_p/(\varepsilon_{cc}/\varepsilon_{co})_e$ are 0.943, 0.042, and 0.047 respectively, which verifies the rationality and reliability of the equation, meanwhile the limitation of the active confinement model lies in its failure to consider the porous characteristics of aggregates, necessitating further investigation in the future [51–53].

4.2. Deformation coordination and equilibrium conditions

At initial loading phase, it is thought that core concrete and steel tube are separated and confining stress of steel tube to core concrete is

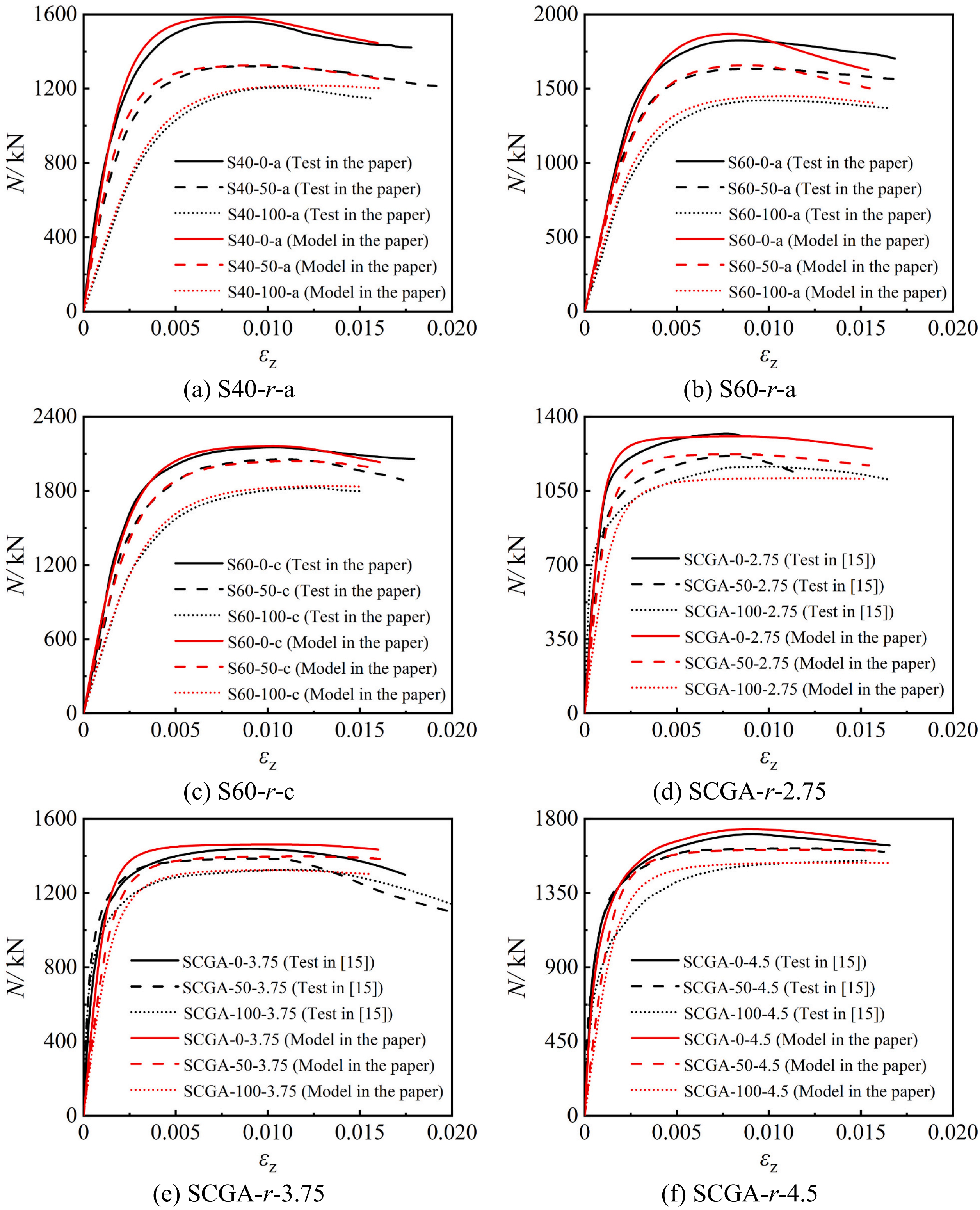

Fig. 10. Comparison of axial load-axial strain curves between experimental measurements and model predictions.

assumed to be zero. Subsequently, as the splitting crack forms, the hoop strain of core concrete increases rapidly to that of steel tube, which begins to confine the core concrete at this time. During this stage, confining stress can be calculated using deformation coordination and equilibrium condition, expressed as:

$$\sigma_r = -\frac{2t}{D-2t}\sigma_{\theta,s} = -\frac{2(t/D)}{1-2(t/D)}\sigma_{\theta,s} \tag{19}$$

4.3. Implementation of the analysis-oriented model

The complete flowchart of the analysis-oriented model for SCGCA CFST specimens proposed in the paper is illustrated in Fig. 9 and described in detail as follows:

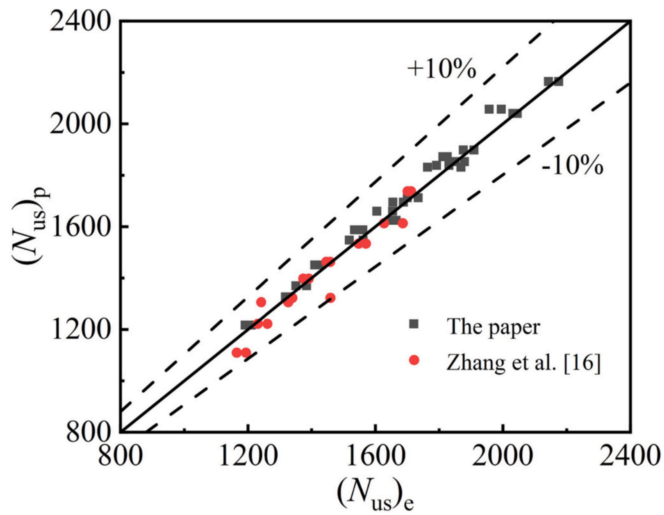

Fig. 11. Comparison of axial bearing capacity between experimental measurements and model predictions.

(1) Input the basic parameters of specimens, such as the section diameter (D), the steel yield strength (f_y) and the steel tube thickness (t) of SCGCA CFST specimens; the peak stress (f'_{co}) of the NCA concrete specimens and SCGCA replacement ratio (r). The f_{co}, ε_{co}, and E_{co} can be calculated by Eqs. (4)–(6). And then, apply an incremental axial strain ($d\varepsilon_z$) of 0.0001 to axial strains of concrete and steel tube which start from 0.

(2) It is assumed that confining stress is zero before axial strain achieves ε_{sc}. The ε_{sc} can be obtained by Eq. (9) under $\sigma_r = 0$. Calculate hoop strains of steel tube ($\varepsilon_{\theta,s}$) and core concrete (ε_x^e) of SCGCA CFST specimens using Eqs. (1)–(3) and (7), (19) respectively. Then the process enters the next step when $\varepsilon_x^e \geq \varepsilon_{\theta,s}$; conversely, adjust axial strain of steel tube and concrete until satisfying the condition.

(3) Continue to apply $d\varepsilon_z$ and calculate the confining stress (σ_r) and hoop strain (ε_x^T) of SCGCA CFST specimens based on the stress-strain model of the steel tube (Eqs. (1)–(3)), the hoop strain-axial strain model of core concrete (Eqs. (7)–(10)) and the deformation coordination and equilibrium conditions (Eq. (19)).

(4) Substitute σ_r and the current axial strain (ε_z) to evaluate axial stresses of core concrete (σ_z^T) in SCGCA CFST specimens based on Eqs. (15)–(18). Acquire axial stresses of steel tube ($\sigma_{z,s}$) by using incremental axial and hoop strains gained from step (3). Furthermore, calculate axial load of the SCGCA CFST specimens (N) by the following equation:

$$N = \sigma_{z,s}A_s + \sigma_z^T A_c \tag{20}$$

where A_s and A_c represent the cross-sectional areas of steel tube and core

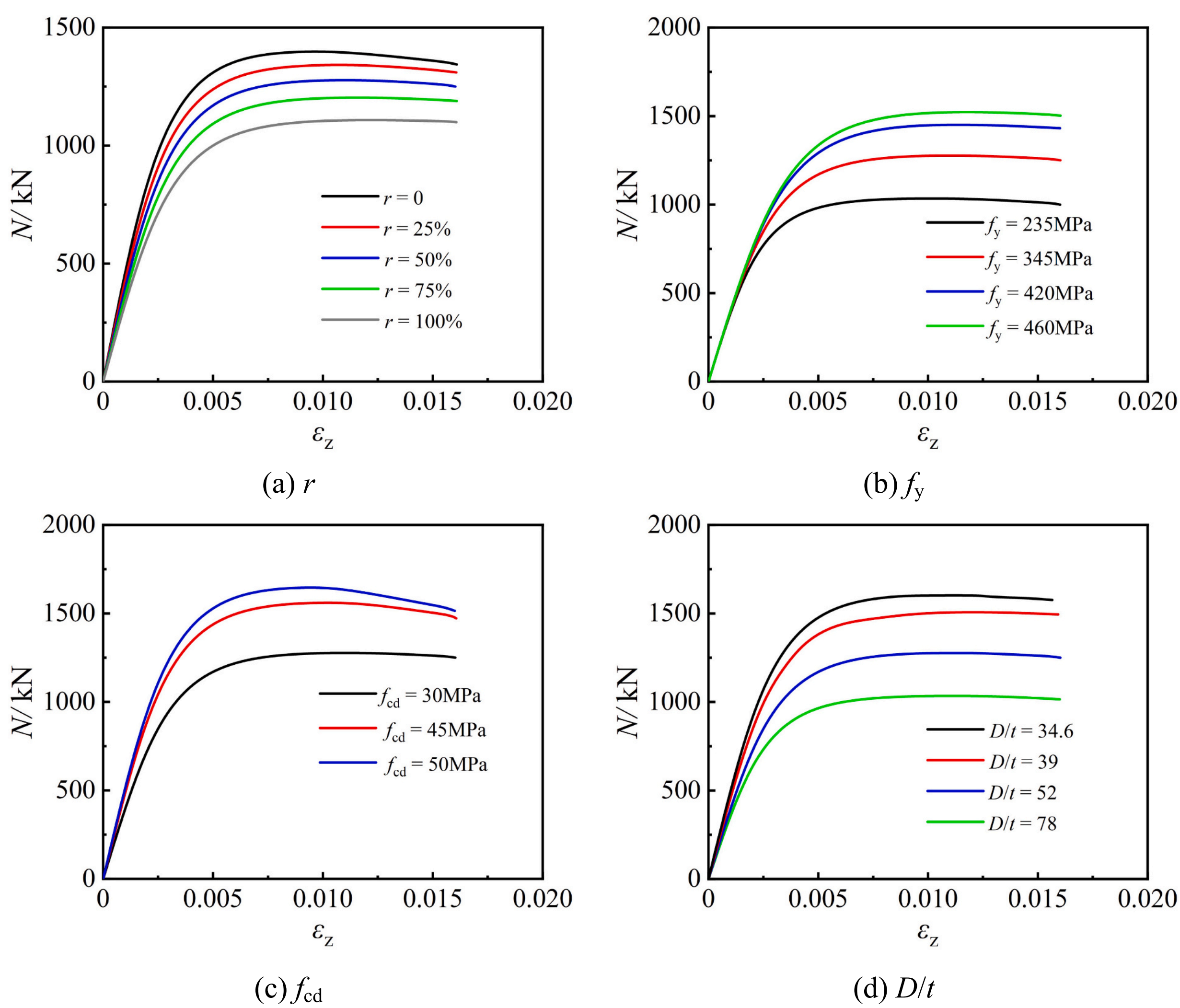

Fig. 12. Effects of critical parameters on N-ε_z curves of the SCGCA CFST stub columns.

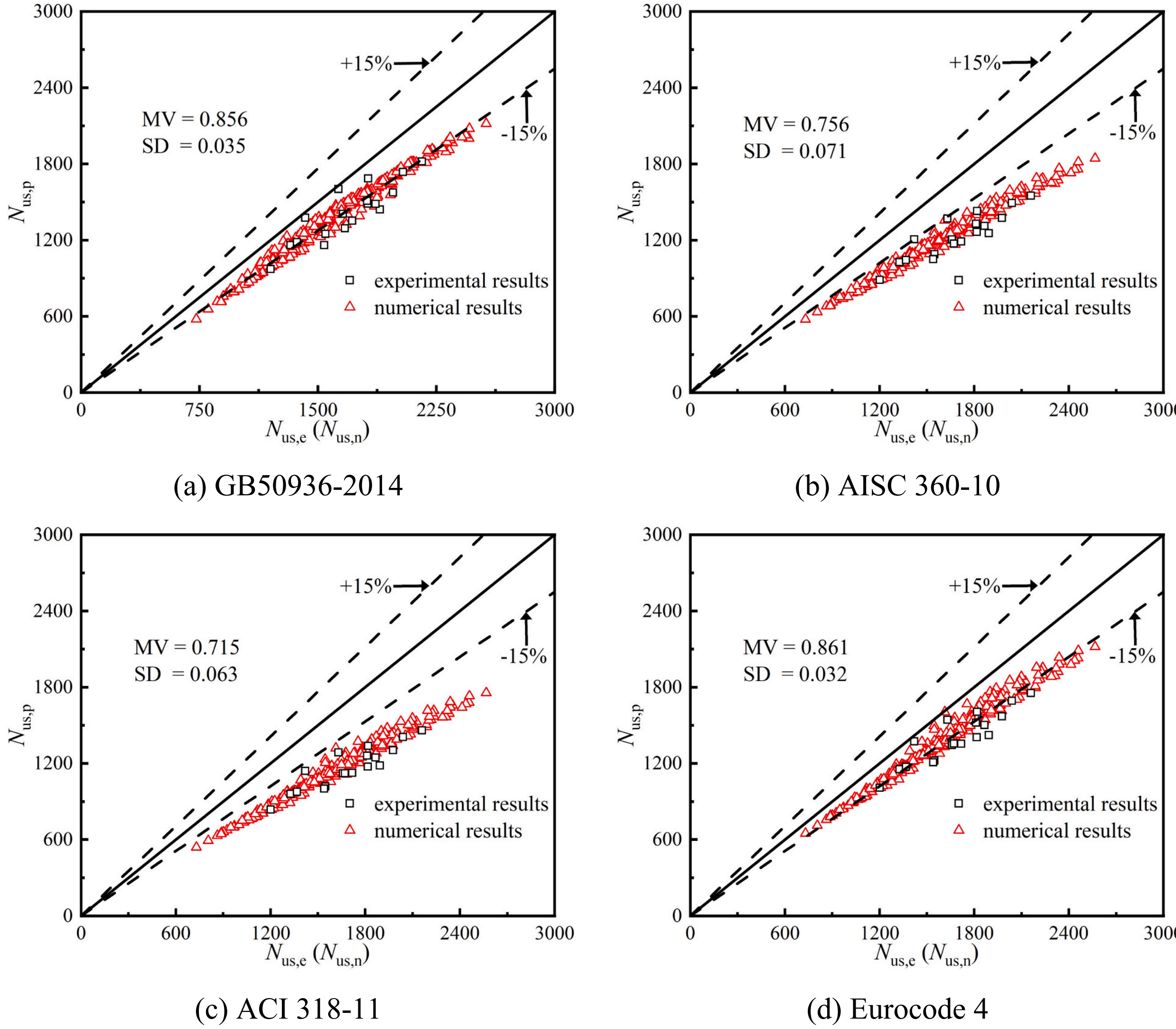

Fig. 13. Evaluations of N_{us} by available design methods in current design codes.

concrete in SCGCA CFST specimens, respectively.

(5) Repeat above steps until total axial strain of core concrete reaches 1.6% and then output complete axial load-axial strain curve of SCGCA CFST specimens.

4.4. Verification of analysis-oriented model

The comparison of axial load (N)-axial strain (ε_z) curves of SCGCA CFST specimens between predicted results by the analysis-oriented model in this paper and tested results is shown in Fig. 10, where the black and red lines represent tested and predicted results, respectively. It can be observed that there is a similar changing trend between the predicted and the tested N-ε_z curves of the SCGCA CFST specimens. Fig. 11 further demonstrates the comparison of axial bearing capacity of SCGCA CFST specimens between predicted results by the analysis-oriented model in the paper and the tested results, where $(N_{us})_p$ and $(N_{us})_e$ are the predicted and tested bearing capacity respectively. It can be obtained that the MV, SD and AAE of $(N_{us})_p/(N_{us})_e$ are 1.002, 0.057, and 0.047 respectively, which verifies the rationality and reliability of analysis-oriented model presented in this paper for SCGCA CFST specimens.

4.5. Extensive parameter analysis

Considering the limited number of tested SCGCA CFST specimens, an extensive parameter analysis was further performed by the proposed analysis-oriented model. The basic conditions of the typical calculation example are: $L = 450$ mm, $D = 156$ mm, $D/t = 52$, $f_y = 345$ MPa, $f_{cd} = 30$ MPa, $r = 50\%$, and the variation ranges of critical parameters are: $r =$ 0–100%, $f_y =$ 235–460 MPa, $f_{cd} =$ 30–50 MPa, $D/t =$ 34.6–78.

Fig. 12 depicts the influences of critical parameters on axial load (N)-axial strain (ε_z) curves of SCGCA CFST stub column. It is observed that initial elastic modulus of N-ε_z curves declines with increasing r and D/t and decreasing f_{cd}, the plastic stage of N-ε_z curves occurs in advance with increasing r and D/t and decreasing f_y and f_{cd}, and the bearing capacity (N_{us}) of SCGCA CFST stub column ascends with decreasing r and D/t and increasing f_y and f_{cd}.

4.6. Verification of the design methods

The reliability of design methods in GB50936–2014 [54], AISC 360–10 [55], ACI 318–11 [56] and Eurocode 4 [57] was discussed for calculating bearing capacity (N_{us}) of SCGCA CFST stub columns under axial compression. The comparison between predicted and experimental or numerical bearing capacities is depicted in Fig. 13, where $N_{us,p}$ and $N_{us,e}$ ($N_{us,n}$) are the predicted and the experimental (numerical) results respectively. It can be obtained that the MV (SD) of $N_{us,p}/N_{us,e/n}$ are 0.856 (0.035), 0.756 (0.071), 0.715 (0.063) and 0.861(0.032) for GB50936–2014, AISC 360–10, ACI 318–11 and Eurocode 4 respectively, which indicates that design approaches in four design codes underestimate bearing capacity of SCGCA CFST stub column subjected to axial compression.

5. Conclusions

On basis of the experimental and theoretical studies in this research, the main conclusions can be made as follows:

(1) Similar to NAC CFST, the outward bulking of steel tube occurs at the end and mid-height of the SCGCA CFST specimens. With the increase of t, the failure modes of specimens change from the shear failure to the drum-like failure; with the increase of r, the damage of core concrete and outward buckling of steel tube tend to be severe.
(2) With the increase of r, the bearing capacity N_{us} and axial splitting strain ε_{csc} of the SCGCA CFST specimens decrease while the peak strain ε_{cc} increases; with the increase of t, the N_{us}, ε_{csc} and ε_{cc} of the SCGCA CFST specimens increase.
(3) Under same axial strain, the hoop strain of SCGCA CFST specimens increases with increasing r, which causes greater circumferential expansion of core concrete and corresponding higher confining stress of steel tube.
(4) The analysis-oriented model developed in this paper, which considers the expansion characteristic of the SCGCA concrete, can reasonably predict mechanical behavior of SCGCA CFST stub columns under axial compression and offer a theoretical guideline for design method and specification of such stub columns.

CRediT authorship contribution statement

Jinli Wang: Conceptualization, Methodology, Writing – original draft, Funding acquisition. **Yongxu Duan:** Data curation, Formal analysis, Writing – review & editing. **Xuetao Lyu:** Investigation, Software, Writing – review & editing. **Yang Yu:** Investigation, Supervision, Validation, Writing – review & editing. **Jiaxuan Xiao:** Data curation, Validation, Writing – review & editing.

Declaration of competing interest

The authors declare that they have no known competing financial interests or personal relationships that could have appeared to influence the work reported in this paper.

Data availability

Data will be made available on request.

Acknowledgements

This study is financially supported by the Scientific Research Fund of Liaoning Provincial Education Department (CN) (LJ2020JCL030), and the discipline innovation team of Liaoning Technical University (CN) (LNTU20TD-12).

References

[1] N. Zhang, H. Li, X. Liu, Hydration mechanism and leaching behavior of bauxite-calcination-method red mud-coal gangue based cementitious materials, J. Hazard. Mater. 314 (2016) 172–180, https://doi.org/10.1016/j.jhazmat.2016.04.040.
[2] X.Y. Cong, S. Lu, Y. Yao, Z. Wang, Fabrication and characterization of self-ignition coal gangue autoclaved aerated concrete, Mater. Des. 97 (2016) 155–162, https://doi.org/10.1016/j.matdes.2016.02.068.
[3] B. Jabłońska, A.V. Kityk, M. Busch, P. Huber, The structural and surface properties of natural and modified coal gangue, J. Environ. Manag. 190 (2017) 80–90, https://doi.org/10.1016/j.jenvman.2016.12.055.
[4] Q. Tang, L. Li, S. Zhang, et al., Characterization of heavy metals in coal gangue-reclaimed soils from a coal mining area, J. Geochem. Explor. 186 (2018) 1–11, https://doi.org/10.1016/j.gexplo.2017.11.018.
[5] X. Zhang, G. Zhou, X. Liu, Y. Fan, E. Meng, J. Yang, Y. Huang, Experimental and numerical analysis of seismic behaviour for recycled aggregate concrete filled circular steel tube frames, Comput. Concr. 31 (6) (2023) 537, https://doi.org/10.12989/cac.2023.31.6.537.
[6] X. Zhang, X. Liu, S. Zhang, J. Wang, L. Fu, J. Yang, Y. Huang, Analysis on displacement-based seismic design method of recycled aggregate concrete-filled square steel tube frame structures, Struct. Concr. (2023), https://doi.org/10.1002/suco.202200720.
[7] C. Ren, J. Yu, X. Liu, Z. Zhang, Y. Cai, Cyclic constitutive equations of rock with coupled damage induced by compaction and cracking, Int. J. Min. Sci. Technol. 32 (5) (2022) 1153–1165, https://doi.org/10.1016/j.ijmst.2022.06.010.
[8] J. Cai, J. Pan, G. Li, M. Elchalakani, Behaviors of eccentrically loaded ECC-encased CFST columns after fire exposure, Eng. Struct. 289 (2023) 116258, https://doi.org/10.1016/j.engstruct.2023.116258.
[9] M. Zhou, Y. Dou, Y. Zhang, et al., Effects of the variety and content of coal gangue coarse aggregate on the mechanical properties of concrete, Constr. Build. Mater. 220 (2019) 386–395, https://doi.org/10.1016/j.conbuildmat.2019.05.176.
[10] Q. Wang, Z. Li, Y. Zhang, et al., Influence of coarse coal gangue aggregates on elastic modulus and drying shrinkage behaviour of concrete, J. Build. Eng. 32 (2020) 101748, https://doi.org/10.1016/j.jobe.2020.101748.
[11] C.X. Dong, A.K.H. Kwan, J.C.M. Ho, Effects of external confinement on structural performance of concrete-filled steel tubes, J. Constr. Steel Res. 132 (2017) 72–82, https://doi.org/10.1016/j.jcsr.2016.12.024.
[12] H.H. Wong, A.K. Kwan, Packing density of cementitious materials: part 1—measurement using a wet packing method, Mater. Struct. 41 (2008) 689–701, https://doi.org/10.1617/s11527-007-9274-5.
[13] Y. Zhang, Q. Wang, M. Zhou, et al., Mechanical properties of concrete with coarse spontaneous combustion gangue aggregate (SCGA): experimental investigation and prediction methodology, Constr. Build. Mater. 255 (2020) 119337, https://doi.org/10.1016/j.conbuildmat.2020.119337.
[14] Q. Wang, Z. Li, M. Zhou, et al., Effects of spontaneous-combustion coal gangue aggregate (SCGA) replacement ratio on flexural behavior of SCGA concrete beams, J. Build. Struc. 41 (2020) 0172, https://doi.org/10.14006/j.jzjgxb.2020.0172.
[15] H. Liu, G. Bai, Y. Gu, F. Yan, The influence of coal gangue coarse aggregate on the mechanical properties of concrete columns, Case Stud. Constr. Mater. 17 (2022) e01315, https://doi.org/10.1016/j.cscm.2022.e01315.
[16] J. Wang, J. Xia, H. Chang, et al., The axial compressive experiment and analytical model for FRP-confined gangue aggregate concrete, Structures 36 (2022) 98–110, https://doi.org/10.1016/j.istruc.2021.12.013.
[17] H. Guan, K. Wang, C.J. Kahwa, Compressive behaviors of FRP-confined concrete prepared using spontaneous combustion gangue as coarse aggregate, Constr. Build. Mater. 376 (2023) 131044, https://doi.org/10.1016/j.conbuildmat.2023.131044.
[18] H. Zhao, T. Ren, A. Remennikov, Behaviour of FRP-confined coal reject concrete columns under axial compression, Compos. Struct. 262 (2021) 113621, https://doi.org/10.1016/j.compstruct.2021.113621.
[19] L. Yu, J. Xia, Z. Xia, et al., Axial compressive behavior of basalt and carbon FRP-confined coal gangue concrete, Constr. Build. Mater. 371 (2023) 130803, https://doi.org/10.1016/j.conbuildmat.2023.130803.
[20] S. Gao, G. Zhao, L. Guo, et al., Utilization of coal gangue as coarse aggregates in structural concrete, Constr. Build. Mater. 268 (2021) 121212, https://doi.org/10.1016/j.conbuildmat.2020.121212.
[21] Y. Zhang, Q. Xu, Q. Wang, et al., Axial compressive behavior of circular concrete-filled steel tube stub columns prepared with spontaneous-combustion coal gangue aggregate, J. Build. Eng. 48 (2022) 103987, https://doi.org/10.1016/j.jobe.2021.103987.
[22] F. Wu, L. Xu, Y. Zeng, et al., Behavior of CA-UHPC filled circular steel tube stub columns under axial compression, J. Constr. Steel Res. 211 (2023) 108204, https://doi.org/10.1016/j.jcsr.2023.108204.
[23] D. Yang, F. Liu, Y. Wang, Axial compression behaviour of rectangular recycled aggregate concrete-filled steel tubular stub columns, J. Constr. Steel Res. 201 (2022) 107687, https://doi.org/10.1016/j.jcsr.2022.107687.
[24] Z. Liu, D. Huang, H. Wu, et al., Axial compressive behavior of steel fiber reinforced concrete-filled square steel tube stub columns. Axial compressive behavior of steel fiber reinforced concrete-filled square steel tube stub columns, J. Constr. Steel Res. 203 (2023) 107804, https://doi.org/10.1016/j.jcsr.2023.107804.
[25] G. Li, Z. Liu, L. Yang, The constitutive equation and strength criterion on core concrete of gangue concrete-filled steel tube, J. Northeast Univ. Nat. Sci. 23 (1) (2002) 64–66.
[26] G. Li, S.T. Zhong, Strength and transverse deformation coefficient of coal gangue concrete confined by steel tube, J. Harbin Univ. Civ. Eng. Archit. 35 (3) (2002) 20–23.
[27] A.K.H. Kwan, C.X. Dong, J.C.M. Ho, Axial and lateral stress–strain model for concrete-filled steel tubes, J. Constr. Steel Res. 122 (2016) 421–433, https://doi.org/10.1016/j.jcsr.2016.03.031.
[28] X. Yu, Z. Tao, T.-Y. Song, Effect of different types of aggregates on the performance of concrete-filled steel tubular stub columns, Mater. Struct. 49 (2016) 3591–3605, https://doi.org/10.1617/s11527-015-0742-z.
[29] Ministry of Housing and Urban-Rural Development of the People's Republic of China, Standard for Technical Requirements and Test Method of Sand and Crushed Stone (Or Gravel) for Ordinary Concrete. JGJ52–2006, Beijing, China, 2006.

[30] China Association for Engineering Construction Standardization, Pebble and Crushed Stone for Construction. GB/T 14685–2011, Beijing, China, 2011.
[31] China Association for Engineering Construction Standardization, Sand for Construction. GB/T 14684–2011, Beijing, China, 2011.
[32] China Association for Engineering Construction Standardization, Metallic Materials—Tensile Testing—Part: 1 Method of Test at Room Temperature. GB/T 228.1–2021, Beijing, China, 2021.
[33] Ministry of Housing and Urban-Rural Development of the People's Republic of China, Specification for mix proportion design of ordinary concrete. JGJ 55–2011, Beijing, China, 2011.
[34] L. Yu, J. Xia, Z. Xia, et al., Study on the mechanical behavior and micro-mechanism of concrete with coal gangue fine and coarse aggregate, Constr. Build. Mater. 338 (2022) 127626, https://doi.org/10.1016/j.conbuildmat.2022.127626.
[35] Ministry of Housing and Urban-Rural Development of the People's Republic of China, Standard for test methods of concrete physical and mechanical propertie. GB/T 50081–2019, Beijing, China, 2019.
[36] W.-Q. Lyu, L.-H. Han, C. Hou, Axial compressive behaviour and design calculations on recycled aggregate concrete-filled steel tubular (RAC-FST) stub columns, Eng. Struct. 241 (2021) 112452, https://doi.org/10.1016/j.engstruct.2021.112452.
[37] B. Han, T.-Y. Xiang, Axial compressive stress-strain relation and Poisson effect of structural lightweight aggregate concrete, Constr. Build. Mater. 146 (2017) 338–343, https://doi.org/10.1016/j.conbuildmat.2017.04.101.
[38] M.H. Lai, J.C.M. Ho, A theoretical axial stress-strain model for circular concrete-filled-steel-tube columns, Eng. Struct. 125 (2016) 124–143, https://doi.org/10.1016/j.engstruct.2016.06.048.
[39] C.R. Calladine, Plasticity for Engineers, Ellis Worwood, New York, Halsted Press, Chichrster, West Sussex, England, 1985.
[40] P. Chen, Y. Wang, C. Liu, Confinement path-dependent analytical model for FRP-confined concrete and concrete-filled steel tube subjected to axial compression, Compos. Struct. 201 (2018) 234–247, https://doi.org/10.1016/j.compstruct.2018.06.008.
[41] J. Yu, Y. Zhu, W. Yao, X. Liu, C. Ren, Y. Cai, X. Tang, Stress relaxation behaviour of marble under cyclic weak disturbance and confining pressures, Measurement 182 (2021) 109777, https://doi.org/10.1016/j.measurement.2021.109777.
[42] C. Ren, J. Yu, S. Liu, W. Yao, Y. Zhu, X. Liu, A plastic strain-induced damage model of porous rock suitable for different stress paths, Rock Mech. Rock. Eng. 55 (4) (2022) 1887–1906, https://doi.org/10.1007/s00603-022-02775-1.
[43] M.H. Lai, S.A.M. Binhowimal, A.M. Griffith, L. Hanzic, Q. Wang, Z. Chen, J.C. M. Ho, Shrinkage design model of concrete incorporating wet packing density, Constr. Build. Mater. 280 (2021) 122448, https://doi.org/10.1016/j.conbuildmat.2021.122448.
[44] M.H. Lai, S.A.M. Binhowimal, A.M. Griffith, L. Hanzic, Z. Chen, Q. Wang, J.C. M. Ho, Shrinkage, cementitious paste volume, and wet packing density of concrete, Struct. Concr. 23 (1) (2022) 488–504, https://doi.org/10.1002/suco.202000407.
[45] J.C.M. Ho, X.L. Ou, M.T. Chen, Q. Wang, M.H. Lai, A path dependent constitutive model for CFFT column, Eng. Struct. 210 (2020) 110367, https://doi.org/10.1016/j.engstruct.2020.110367.
[46] M.H. Lai, Y.W. Liang, Q. Wang, F.M. Ren, M.T. Chen, J.C.M. Ho, A stress-path dependent stress-strain model for FRP-confined concrete, Eng. Struct. 203 (2020) 109824, https://doi.org/10.1016/j.engstruct.2019.109824.
[47] M.H. Lai, W. Song, X.L. Ou, M.T. Chen, Q. Wang, J.C.M. Ho, A path dependent stress-strain model for concrete-filled-steel-tube column, Eng. Struct. 211 (2020) 110312, https://doi.org/10.1016/j.engstruct.2020.110312.
[48] M.M. Attard, S. Setunge, Stress-strain relationship of confined and unconfined concrete, ACI Mater. J. 93 (5) (1996) 432–442.
[49] Q.G. Xiao, J.G. Teng, T. Yu, Behavior and modeling of confined high-strength concrete, J. Compos. Constr. 14 (2010) 249–259, https://doi.org/10.1061/(ASCE)CC.1943-5614.0000070.
[50] J.C. Lim, T. Ozbakkaloglu, Stress–strain model for normal- and light-weight concretes under uniaxial and triaxial compression, Constr. Build. Mater. 71 (2014) 492–509, https://doi.org/10.1016/j.conbuildmat.2014.08.050.
[51] A.K.H. Kwan, C.X. Dong, J.C.M. Ho, Axial and lateral stress–strain model for FRP confined concrete, Eng. Struct. 99 (2015) 285–295, https://doi.org/10.1016/j.engstruct.2015.04.046.
[52] C.X. Dong, A.K.H. Kwan, J.C.M. Ho, A constitutive model for predicting the lateral strain of confined concrete, Eng. Struct. 91 (2015) 155–166, https://doi.org/10.1016/j.engstruct.2015.02.014.
[53] M. Lai, L. Hanzic, J.C. Ho, Fillers to improve passing ability of concrete, Struct. Concr. 20 (1) (2019) 185–197, https://doi.org/10.1002/suco.201800047.
[54] Ministry of Housing and Urban-Rural Development of the People's Republic of China, Technical Code for Concrete Filled Steel Tubular Structures. GB50936–2014, Beijing, China, 2014.
[55] American Institute of Steel Construction, Specification for Structural Steel Building. AISC 360–10, Chicago, Illinois, USA, 2010.
[56] American Concrete Insitute, Building Code Requirements for Structural Concrete and Commentary. ACI 318-11, Farmington Hills, MI, USA, 2011.
[57] European Committee for Standardization, Design of Composite Steel and Concrete Structures – Part 1–1: General Rules for Buildings. Eurocode 4, Brussels, Belgium, 2004.